ACS APPLIED MATERIALS & INTERFACES

www.acsami.org

Research Article

A "MOFs plus ZIFs" Strategy toward Ultrafine Co Nanodots Confined into Superficial N-Doped Carbon Nanowires for Efficient Oxygen Reduction

Jinshuai Liu, Hao Zhang, Jiashen Meng, Chunhua Han,* Fang Liu, Xiong Liu, Peijie Wu, Ziang Liu, Xuanpeng Wang, and Liqiang Mai*

Cite This: https://dx.doi.org/10.1021/acsami.0c14112

Read Online

ACCESS | Metrics & More | Article Recommendations | Supporting Information

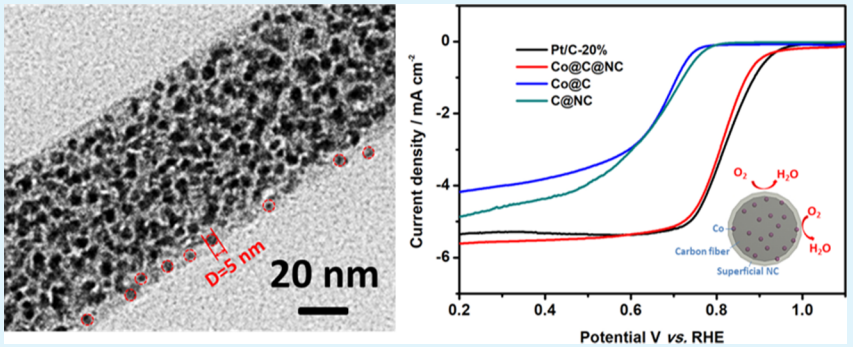

ABSTRACT: N-doped carbon-confined transition metal nanocatalysts display efficient oxygen reduction reaction (ORR) performance comparable to commercial Pt/C electrocatalysts because of their efficient charge transfer from metal atoms to active N sites. However, the sheathed active sites inside the electrocatalysts and relatively large-size confined metal particles greatly restrict their activity improvement. Here, we develop a facile and efficient "MOFs plus ZIFs" synthesis strategy to successfully construct ultrafine sub-5 nm Co nanodots confined into superficial N-doped carbon nanowires (Co@C@NC) via a well-designed synthesis process. The unique synthesis mechanism is based on low-pressure vapor superassembly of thin zeolitic imidazolate framework (ZIF) coatings on metal−organic framework substrates. During the successive pyrolysis, the preferential formation of the robust N-doped carbon shell from the ZIF-67 shell keeps the core morphology without shrinkage and limits the growth of Co nanodots. Benefiting from this architecture with accessible and rich active N sites on the surface, stable carbon confined architecture, and large surface area, the Co@C@NC exhibits excellent ORR performance, catching up to commercial Pt/C. Density functional theory demonstrates that the confined Co nanodots efficiently enhance the charge density of superficial active N sites by interfacial charge transfer, thus accelerating the ORR process.

KEYWORDS: *low-pressure vapor superassembly, MOF composite design, superficial N-doped carbon, nanowires, oxygen reduction*

1. INTRODUCTION

The oxygen reduction reaction (ORR) is of crucial importance in sustainable energy storage and conversion devices, including fuel cells and metal-air batteries.[1−3] The materials based on Pt are the benchmark ORR catalysts, but their practical applications are constrained by the scarcity, high cost, and poor stability.[4−6] Developing efficient nonprecious metal-based catalysts is desirable to replace the catalysts based on Pt.[7−9] However, the performance of these catalysts is mainly limited by their intrinsic activity and accessible number of active sites.[10] To obtain catalysts with high intrinsic active sites, a variety of nonprecious metal-based materials have been explored. Among them, the catalysts based on transition metal/metal carbide/metal oxide nanoparticles encapsulated in nanostructured N-doped carbon (M@NC, M = Fe, Co, Cu, etc.) have been widely studied in which the accessible surface N boosted by transition metal is considered as the active site.[11] Wang et al. reported Fe/Fe_3C nanoparticles encapsulated in N-doped graphene and carbon nanotubes with N active sites boosted by Fe.[12] To further enhance ORR performance, increasing accessible active sites of M@NC is believed to be a key factor. Generally, the architecture of these catalysts is always determined by the morphology and structure of

Received: August 5, 2020
Accepted: November 4, 2020

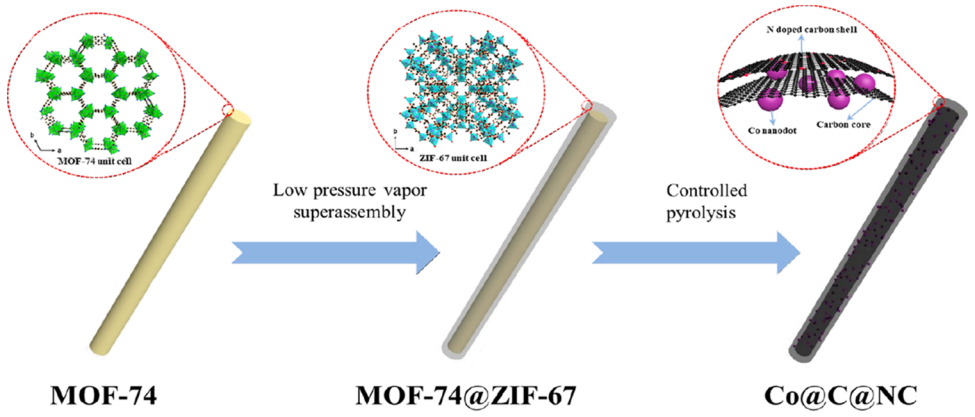

Figure 1. Schematic illustration of the synthesis process and structure of Co@C@NC.

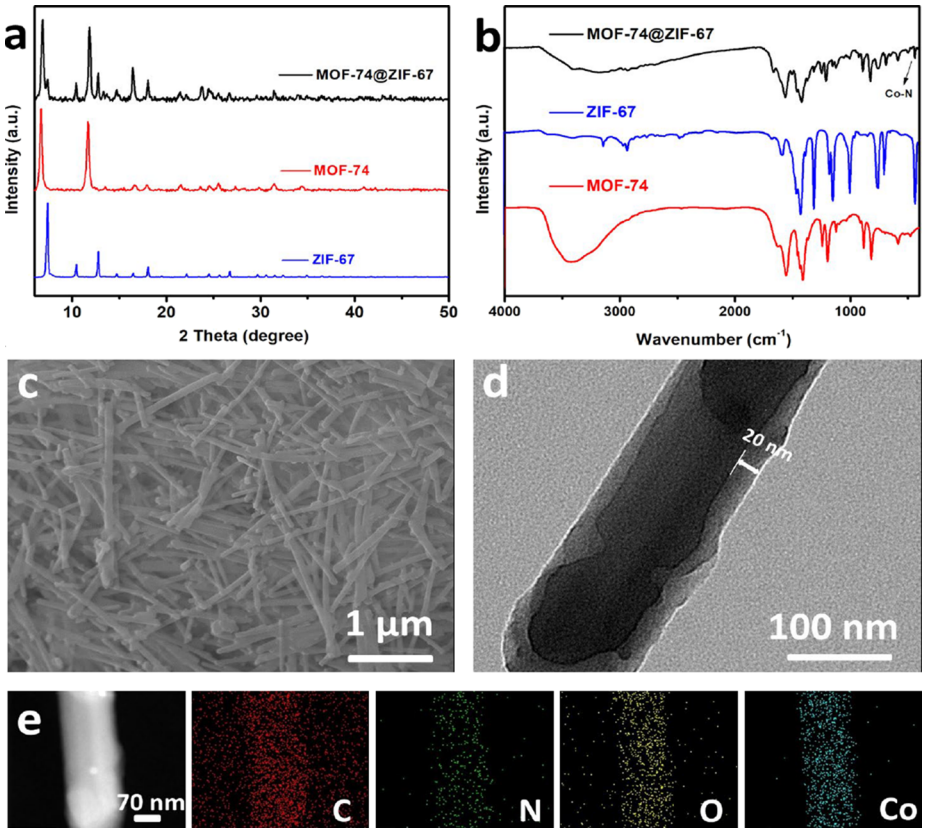

Figure 2. (a) XRD patterns of MOF-74, ZIF-67, and MOF-74@ZIF-67 nanowires. (b) FTIR spectra of MOF-74, ZIF-67, and MOF-74@ZIF-67 nanowires. (c) SEM image, (d) TEM image, and (e) HAADF-STEM image with the corresponding EDS element mapping of the MOF-74@ZIF-67 nanowire.

precursors. Therefore, it is essential to design suitable precursors to synthesize M@NC catalysts with a high surface area and rich accessible active sites.[13,14]

Metal−organic frameworks (MOFs) are porous crystal compounds assembled from metal ions/clusters coordinated with organic ligands.[15−18] Benefiting from the fantastic properties of controllable architecture and high surface area, MOFs have been considered to be promising precursors for fabricating M@NC catalysts with high surface area and tunable surface properties.[19−22] Lai et al. reported controllable Cu@NC nanocatalysts by annealing adjustable Cu-zeolitic imidazolate framework (ZIF)-8 nanoparticles.[23] Zhang et al. designed CoFe@NC hollow spheres by pyrolyzing MIL-101/ZIF-67 composites.[24] As expected, these M@NC catalysts achieved a high specific surface area. However, because of homogeneous N doping in MOF precursors during the synthesis process, the M@NC catalysts derived from these MOFs have doped N sites through the whole carbon materials.[25,26] Despite some accessible N sites activated on the surface, most N sites are deeply sheathed without accessibility because the ORR is performed on the surface.[27] In addition, most these catalysts have relatively large metal particles (>10 nm), further reducing the accessible active sites on the surface.[28] So far, it is still necessary to develop a suitable strategy to design M@NC catalysts with ultrafine metal

https://dx.doi.org/10.1021/acsami.0c14112
ACS Appl. Mater. Interfaces XXXX, XXX, XXX−XXX

nanodots confined and most accessible active N sites focusing on the surface.

Herein, a facile "MOFs plus ZIFs" strategy following controlled pyrolysis has been developed to design a new type of ultrafine sub-5 nm Co nanodots confined into superficial N-doped carbon nanowires (Co@C@NC). This "MOFs plus ZIFs" strategy achieves the uniform growth of thin ZIF-67 coating on MOF-74. The preferential pyrolysis of ZIF-67 can generate stable N-doped carbon shells and hinder the growth of Co nanodots. Benefiting from the well-designed process, the resultant Co@C@NC can simultaneously achieve a high surface area and rich accessible active sites doping on the surface. The as-prepared catalyst exhibits high catalytic activity in alkaline electrolyte with a half-wave potential of 0.83 V, catching up to the commercial Pt/C catalyst. The enhanced charge transfer between Co nanodots and N-doped carbon shells is also proved by density functional theory (DFT) calculations.

2. RESULTS AND DISCUSSION

The overall fabrication process of Co@C@NC is shown in Figure 1. MOF-74 nanowires (~70 nm in diameter and ~20 μm in length) (Figure S1) were prepared by the reported hydrothermal method.[29] Then, these nanowires were activated to remove water molecules from the channels and avoid water participating in the subsequent reaction. The activated MOF-74 nanowires and 2-methylimidazole (2-MIM) powders were both placed in a common system and treated at 120 °C under low pressure. Then 2-MIM was converted from solid to gas and filled the entire reaction system. The gaseous 2-MIM ligands reacted with MOF-74 on the surface, forming in situ ZIF-67 shells. During this process, 2-MIM released protons and coordinated with Co^{2+} to form ZIF-67, while the ligands of MOF-74 accepted protons and released 2, 5-dihydroxyparaxic acid (DHTA).[30,31] The reaction equation could be described as follows:

$$2-\mathrm{MIM\,(g)} + \mathrm{MOF-74(s)} \rightarrow \mathrm{MOF-74@ZIF-67(s)} + \mathrm{DHTA(g)} \quad (1)$$

The formation of uniform ZIF-67 shells on MOF-74 nanowires was proved. The X-ray diffraction (XRD) pattern of MOF-74@ZIF-67 revealed typical diffraction peaks corresponding to MOF-74 and ZIF-67 (Figure 2a).[32−34] Fourier transform infrared spectroscopy (FTIR) of MOF-74@ZIF-67 also revealed the feature vibrations of MOF-74 and ZIF-67 (Figure 2b). The adsorption band at 421 cm^{-1} represented the Co−N vibration, indicating that Co^{2+} ions were successfully coordinated with deprotonated 2-MIM.[35] The scanning electron microscopy (SEM) image showed most MOF-74@ZIF-67 maintained the nanowire morphology (Figure 2c). The transmission electron microscopy (TEM) image clearly indicated the core-shell feature of the MOF-74@ZIF-67 nanowire (Figure 2d). The thickness of the uniform ZIF-67 shell is ~20 nm and the diameter of the MOF-74 core remained at ~60 nm. Comparing the diameter of MOF-74 before reaction (~70 nm), it can be estimated that the transformation content of the MOF-74 core in the ZIF-67 shell is ~27%. High-angle annular dark-field scanning TEM (HAADF-STEM) and the corresponding energy-dispersive X-ray spectroscopy (EDS) mapping images of MOF-74@ZIF-67 showed the homogeneous distribution of C, O, N, and Co elements in the overall MOF-74@ZIF-67 (Figure 2e). Therefore, all the above results indicated uniform ZIF-67 shells were formed on the surface of MOF-74.

Co@C@NC was prepared by the controlled pyrolysis of the MOF-74@ZIF-67 precursor in an Ar/H_2 atmosphere. For insight into the morphology evolution after pyrolysis, MOF-74 was directly sintered into Co@C nanowires under the same condition for comparison. The Co@C@NC sample retained the morphology of nanowires in the SEM image (Figure 3a).

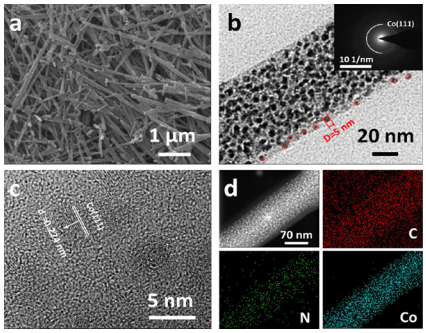

Figure 3. (a) SEM image of Co@C@NC nanowires; (b) TEM image and SAED pattern of a single Co@C@NC nanowire; (c) HRTEM image; and (d) corresponding EDS element mapping of C, N, and Co of Co@C@NC nanowires.

The TEM image revealed the Co@C@NC had a smooth surface with ultrafine Co nanodots uniformly confined (Figure 3b). There was no obvious shrinkage in the Co@C@NC (~100 nm in diameter) compared to the MOF-74@ZIF-67 precursor. However, the surface of Co@C was rough with many protrusions and most large Co particles (>10 nm) were exposed (Figure S2). The diameter of Co@C (~40 nm) had a significant shrinkage compared to that of the MOF-74 precursor (~70 nm). It could be inferred that MOF-74 nanowires suffered from severe collapse during the pyrolysis process, but ZIF-67 had less collapse and provided a relatively stable carbon skeleton to inhibit the growth of Co particles under the same condition. The red dotted circles reflected that the size of most Co nanodots is below 5 nm. These small Co nanodots were expected to boost more accessible N active sites.[36] The diffraction ring in the corresponding selected area electron diffraction (SAED) pattern (inset in Figure 3b) and a lattice fringe space of 0.224 nm in the high-resolution TEM (HRTEM) image (Figure 3c) was attributed to the (111) crystal plane of Co.[37] The EDS element mapping shown in Figure 3d revealed that C and N elements distributed wider than Co, which was more obvious in high magnification (Figure S3), indicating almost all the Co nanodots were coated by superficial N doped C shells. As shown in Figure S4, N elements are mainly distributed at the edges, indicating superficial N doping along the radial direction of Co@C@NC.

To explore the formation mechanism of core-shell Co@C@NC, thermogravimetric (TG) and differential scanning calorimetry (DSC) analyses were performed for MOF-74, MOF-74@ZIF-67, and ZIF-67 (Figure S5). The TG curve of MOF-74@ZIF-67 demonstrated that its mass loss centered on two distinct temperature ranges, including 16% mass loss in 280-400 °C and 17% mass loss in 440−530 °C.[38,39] These two mass losses are the pyrolysis of ZIF-67 and MOF-74, respectively. The DSC curve of MOF-74@ZIF-67 indicated that the exothermic peak position was 460 °C, lower than that of MOF-74 (530 °C), further proving the preferential pyrolysis

https://dx.doi.org/10.1021/acsami.0c14112
ACS Appl. Mater. Interfaces XXXX, XXX, XXX−XXX

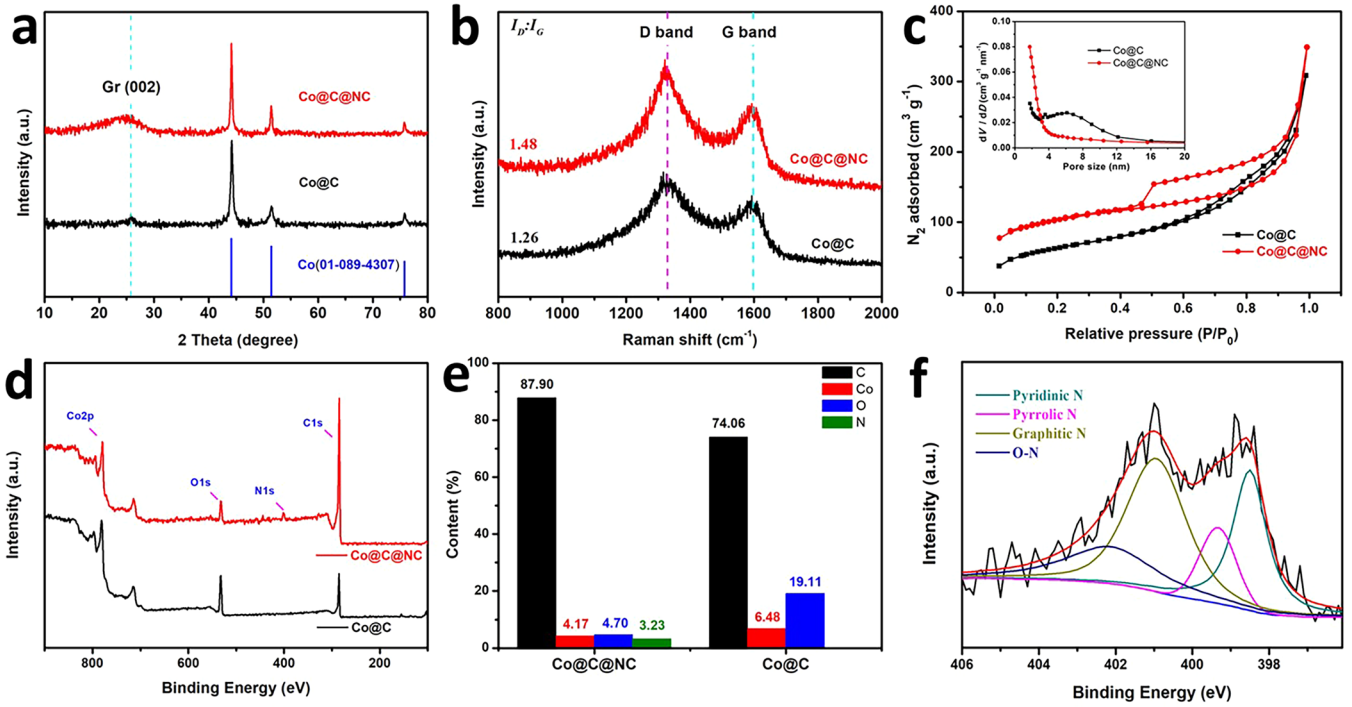

Figure 4. (a) XRD patterns, (b) Raman spectra, (c) N_2 absorption-desorption isotherms with pore size distributions, (d) X-ray photoelectron spectroscopy (XPS) survey spectra, and (e) corresponding element contents of Co@C@NC and Co@C. (f) High-resolution N 1s XPS spectrum of Co@C@NC.

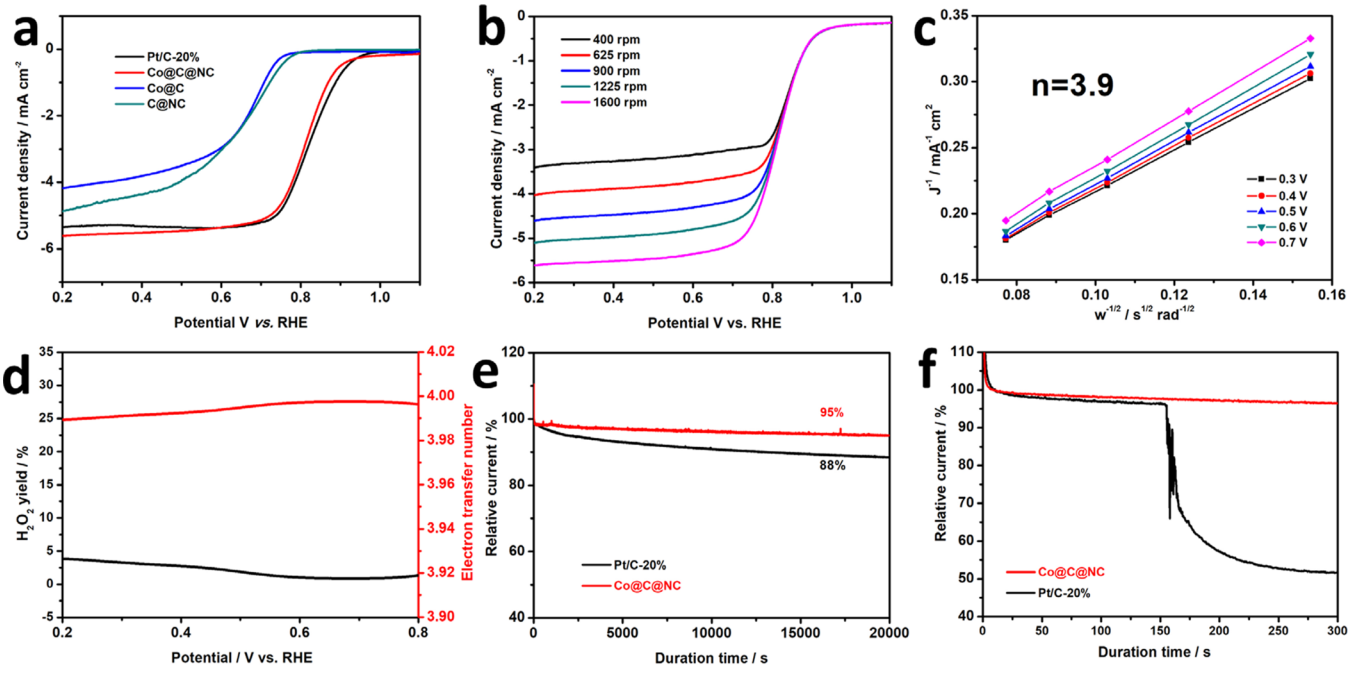

Figure 5. (a) Rotating disk electrode (RDE) polarization curves of the synthesized Co@C@NC, Co@C, and Pt/C-20% at a scan rate of 5 mV s^{-1} and a rotation speed of 1600 rpm; (b) ORR polarization curves and (c) the corresponding K–L plots of the Co@C@NC catalyst at different rotation rates; (d) hydrogen peroxide yield (black) and electron transfer number (red) of Co@C@NC; (e) I-t chronoamperometric response of Co@C@NC and Pt/C-20% at 0.7 V with a rotation rate of 1225 rpm; and (f) chronoamperometric response for the Co@C@NC and Pt/C-20% catalyst at 0.7 V in 0.1 mol L^{-1} KOH (200 mL) solution with the introduction of methanol (0.3 mL). All measures were performed in the O_2-saturated KOH solution.

of the ZIF-67 shell. Combined with different morphologies of Co@C@NC and Co@C, the preferential pyrolysis of the ZIF-67 shell could form a stable and denser N-doped carbon shell on the surface, which inhibited the collapse of the carbon skeleton and limited the growth of Co nanodots.

XRD patterns of both Co@C@NC and Co@C showed sharp peaks at 75.8, 51.5, and 44.2° corresponding to (220),

https://dx.doi.org/10.1021/acsami.0c14112
ACS Appl. Mater. Interfaces XXXX, XXX, XXX−XXX

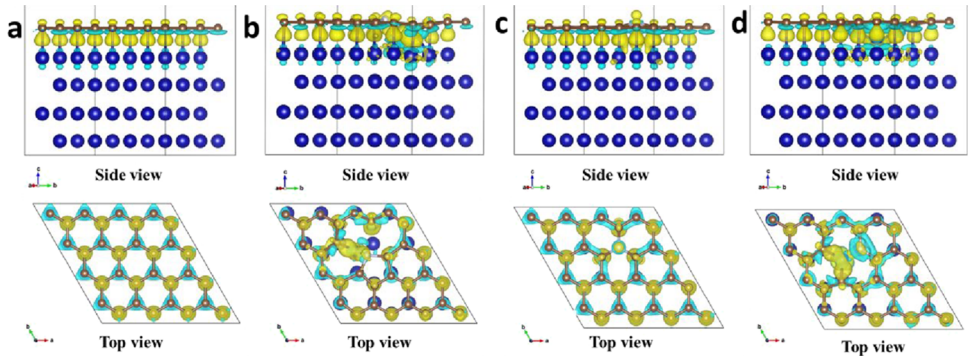

Figure 6. Differential charge density redistributions of (a) Co@C, (b) Co@pyrr-NC, (c) Co@grap-NC, and (d) Co@pyri-NC systems. Atoms with blue, brown, and white represent Co, C, and N atoms. Blue and yellow contours represent charge loss and charge accumulation.

(200), and (111) planes of metallic Co (JCPDS No.: 01-089-4307), respectively (Figure 4a). The broad peak for graphitic carbon (002) at 26.5° in the Co@C@NC pattern showed higher intensity than that in the Co@C pattern, implying a higher graphitization degree of Co@C@NC.[40] The Raman spectroscopy of both samples showed the typical D-band and G-band (Figure 4b). The relative intensity ratio of the D-band and G-band (I_D/I_G) of Co@C@NC was about 1.48, higher than that of Co@C (I_D/I_G = 1.26), indicating that Co@C@NC had more carbon defects on the surface than Co@C.[41] The nitrogen adsorption−desorption isotherm revealed typical IV curves of both samples (Figure 4c).[42] The pore size distribution further confirmed that Co@C contained more mesopores, while Co@C@NC mainly contained micropores (inset of Figure 4c). The Brunauer−Emmett−Teller surface area of Co@C@NC and Co@C was calculated to be 350.9 and 225.7 $m^2\ g^{-1}$, respectively. Consequently, ZIF-67 could produce more micropores and relatively higher specific surface area for the final catalyst than MOF-74 in controlled pyrolysis. The XPS spectrum of Co@C@NC revealed typical peaks of C, Co, N, and O as expected (Figure 4d). Figure 4e shows the content of each element in Co@C@NC and Co@C. The superficial content of Co and N reached as high as 4.17 and 3.23 wt %. Inductively coupled plasma mass spectrometry analysis further showed the total content of Co is 21.3 wt %. This fact indicated that Co nanodots are encapsulated in superficial N-doped carbon. The high-resolution N 1s XPS spectrum of Co@C@NC was deconvoluted into four peaks: pyridine-N (398.5 eV), pyrrole-N (399.3 eV), graphite-N (400.9 eV), and oxidation-N (402.1 eV) (Figure 4f). High contents of graphite-N and pyridine-N in Co@C@NC were considered to promote the adsorption of oxygen and the $4e^-$ reduction.[43] High-resolution Co $2p_{3/2}$ and $2p_{1/2}$ spectra of Co@C@NC could be deconvoluted into metal Co bond and multivalent Co bond (Figure S6). The metal Co stronger energy in Co@C@NC demonstrated that Co nanodots were tightly encapsulated by N-doped carbon.[14,20]

To investigate the ORR activity of Co@C@NC, the linear sweep voltammetry (LSV) was used to evaluate the designed catalyst as shown in Figure 5a. The initial potential (E_{onset}) and half-wave potential ($E_{1/2}$) of Co@C@NC were 0.92 and 0.83 V, respectively, which were close to those of Pt/C (20 wt %). These facts indicated the high ORR activity of the well-designed Co@C@NC catalyst. To prove the location of the active site, Co@C@NC was etched by 25% H_2SO_4 to obtain superficial N-doped carbon nanowires (C@NC) for comparison. The XRD pattern of C@NC revealed no peak of metallic Co (Figure S7a) and few Co nanodots could be found in the TEM image (Figure S7b). Obviously, the reduction potential and current density of the Co@C@NC catalyst were much higher than those of Co@C and C@NC, indicating that the active site is at the N atom boosted by Co nanodots. The electrochemically active surface area of the Co@C@NC catalyst is calculated to be as high as 62.8 mF cm^{-2}, indicating more exposed active sites (Figure S8). Moreover, the catalytic current increased with speed typically in the LSV curves of Co@C@NC (Figure 5b). The corresponding Koutecky−Levich plots indicated that the average electron transfer number (n) was ∼3.9 in the voltage range from 0.3 to 0.7 V (Figure 5c). The ring-shaped RDE examination revealed that the electron transfer number was maintained at 3.99−4.00 in the potential range of 0.2−0.8 V (Figure 5d), consistent with the RDE results. The yield of H_2O_2 did not exceed 4% in the same potential range. The results above suggested that the Co@C@NC catalyst experienced a near $4e^-$ ORR process.[39,44,45] The durability and methanol tolerance of Co@C@NC and Pt/C were compared. The stable current at 10 s was recorded as 100% activity in these examinations. The activity retention rate of Co@C@NC was as high as 95% after 20,000 s, significantly higher than that of Pt/C (88%) (Figure 5e). The TEM image showed that the original morphology of Co@C@NC was maintained after durability examination (Figure S9). In addition, XRD patterns and XPS spectra before and after durability examination further demonstrated the excellent structural stability of Co@C@NC (Figure S10). When methanol was injected to the electrolyte at 150 s, no obvious change was visible in the current density for Co@C@NC, indicating its excellent methanol tolerance (Figure 5f). However, the current density of the Pt/C catalyst was reduced obviously, which was attributed to the catalytic oxidation of methanol.[46] This synthesized Co@C@NC catalyst showed excellent ORR activity compared to similar electrocatalysts reported recently, further illustrating the superiority of the designed structure (Table S1).

To reveal the effect of Co nanodots on N-doped C shells, DFT simulations were used to calculate the charge density redistributions of four systems: Co nanodots encapsulated in N-free, pyrrole-N, pyridine-N, and graphite-N-doped carbon shells (denoted as Co@C, Co@pyrr-NC, Co@pyri-NC, and Co@grap-NC). The introduction of pyrrole-N, pyridine-N, and graphite-N changed the charge density of the Co@C system and accumulated charge at the N sites (Figure 6 a−d). These N-doped systems were more conducive to electron transfer at N sites.[47] Density of states (DOS) was an effective

https://dx.doi.org/10.1021/acsami.0c14112
ACS Appl. Mater. Interfaces XXXX, XXX, XXX−XXX

parameter to analyze the catalytic activity for carbon-based catalysts.[48] In the DOS of spin down, the states near the Fermi level of these four systems were almost consistent (Figure S11a). However, the DOS of spin up showed the systems containing N had more states than Co@C near the Fermi level (Co@pyrr-NC > Co@grap-NC > Co@pyri-NC > Co@C) (Figure S11b). The extra DOS near the Fermi level was expected to enhance the electrochemical activity.[49] The charge density redistribution and the DOS indicated that the local dipoles formed between Co nanodots and external N-doped C shells, which promoted the electron transfer in the ORR process.[50]

3. CONCLUSIONS

In summary, a facile "MOFs plus ZIFs" synthesis strategy was developed to successfully construct a new type of ultrafine sub-5 nm Co@C@NC. The "MOFs plus ZIFs" synthesis mechanism is the in situ growth of a thin ZIF-67 shell on MOF-74 substrates by low-pressure vapor superassembly. Under controlled pyrolysis, the preferential pyrolyzed ZIF-67 can form stable superficial N-doped carbon shells, which inhibit the structural collapse and growth of Co nanodots. Benefiting from the well-designed process, this Co@C@NC catalyst achieves rich and accessible active sites focusing on the surface and high specific surface area, thus exhibiting excellent ORR performance. The experimental and DFT analyses indicate the effects of Co nanodots on N-doped carbon shells. These effects change charge density redistributions and increase the DOS near the Fermi level, enhancing the electron transfer in the ORR process. Considering the diversity of substrates and MOFs, this strategy provides a new direction for the rational design of high-performance catalysts.

■ ASSOCIATED CONTENT

Supporting Information

The Supporting Information is available free of charge at https://pubs.acs.org/doi/10.1021/acsami.0c14112.

Synthesis and characterization of materials; SEM and TEM images of MOF-74 nanowires and Co@C; HAADF-STEM and EDS element mapping of a Co@C@NC nanowire; HAADF-STEM image and N distribution of Co@C@NC; TG-DSC curves; high-resolution XPS spectra; XRD patterns; TEM images; CV curves; spin polarized DOS of all systems; and summary of various similar electrocatalysts reported recently for the ORR (PDF).

■ AUTHOR INFORMATION

Corresponding Authors

Chunhua Han − *State Key Laboratory of Advanced Technology for Materials Synthesis and Processing, Wuhan University of Technology, Wuhan 430070, P. R. China*; Email: hch5927@whut.edu.cn

Liqiang Mai − *State Key Laboratory of Advanced Technology for Materials Synthesis and Processing, Wuhan University of Technology, Wuhan 430070, P. R. China; Foshan Xianhu Laboratory of the Advanced Energy Science and Technology Guangdong Laboratory, Xianhu Hydrogen Valley, Foshan 528200, China;* orcid.org/0000-0003-4259-7725; Email: mlq518@whut.edu.cn

Authors

Jinshuai Liu − *State Key Laboratory of Advanced Technology for Materials Synthesis and Processing, Wuhan University of Technology, Wuhan 430070, P. R. China*

Hao Zhang − *State Key Laboratory of Advanced Technology for Materials Synthesis and Processing, Wuhan University of Technology, Wuhan 430070, P. R. China*

Jiashen Meng − *State Key Laboratory of Advanced Technology for Materials Synthesis and Processing, Wuhan University of Technology, Wuhan 430070, P. R. China*

Fang Liu − *State Key Laboratory of Advanced Technology for Materials Synthesis and Processing, Wuhan University of Technology, Wuhan 430070, P. R. China*

Xiong Liu − *State Key Laboratory of Advanced Technology for Materials Synthesis and Processing, Wuhan University of Technology, Wuhan 430070, P. R. China*

Peijie Wu − *State Key Laboratory of Advanced Technology for Materials Synthesis and Processing, Wuhan University of Technology, Wuhan 430070, P. R. China*

Ziang Liu − *State Key Laboratory of Advanced Technology for Materials Synthesis and Processing, Wuhan University of Technology, Wuhan 430070, P. R. China*

Xuanpeng Wang − *Department of Physical Science & Technology, School of Science, Wuhan University of Technology, Wuhan 430070, P. R. China; Foshan Xianhu Laboratory of the Advanced Energy Science and Technology Guangdong Laboratory, Xianhu Hydrogen Valley, Foshan 528200, China;* orcid.org/0000-0001-6382-4961

Complete contact information is available at: https://pubs.acs.org/10.1021/acsami.0c14112

Author Contributions

J.L. and H.Z. contributed equally to this work.

Notes

The authors declare no competing financial interest.

■ ACKNOWLEDGMENTS

This work was supported by the National Natural Science Foundation of China (51872218, 21905218, and 51832004), the Foshan Xianhu Laboratory of the Advanced Energy Science and Technology Guangdong Laboratory (XHT2020-003), and the Fundamental Research Funds for the Central Universities (WUT: 2020IVB034, 2020IVA036).

■ REFERENCES

(1) Xia, W.; Mahmood, A.; Liang, Z.; Zou, R.; Guo, S. Earth-Abundant Nanomaterials for Oxygen Reduction. *Angew. Chem., Int. Ed.* **2016**, *55*, 2650−2676.

(2) Asset, T.; Atanassov, P. Iron-Nitrogen-Carbon Catalysts for Proton Exchange Membrane Fuel Cells. *Joule* **2020**, *4*, 33−44.

(3) Meng, D.-L.; Chen, C.-H.; Yi, J.-D.; Wu, Q.; Liang, J.; Huang, Y.-B.; Cao, R. Migration-Prevention Strategy to Fabricate Single-Atom Fe Implanted N-Doped Porous Carbons for Efficient Oxygen Reduction. *Research* **2019**, 1768595.

(4) Li, J.-C.; Hou, P.-X.; Zhao, S.-Y.; Liu, C.; Tang, D.-M.; Cheng, M.; Zhang, F.; Cheng, H.-M. A 3D Bi-functional Porous N-doped Carbon Microtube Sponge Electrocatalyst for Oxygen Reduction and Oxygen Evolution Reactions. *Energy Environ. Sci.* **2016**, *9*, 3079−3084.

(5) Cheng, Q.; Yang, L.; Zou, L.; Zou, Z.; Chen, C.; Hu, Z.; Yang, H. Single Cobalt Atom and N Codoped Carbon Nanofibers as Highly Durable Electrocatalyst for Oxygen Reduction Reaction. *ACS Catal.* **2017**, *7*, 6864−6871.

(6) Xu, Y.; Deng, P.; Chen, G.; Chen, J.; Yan, Y.; Qi, K.; Liu, H.; Xia, B. Y. 2D Nitrogen-Doped Carbon Nanotubes/Graphene Hybrid as Bifunctional Oxygen Electrocatalyst for Long-Life Rechargeable Zn−Air Batteries. *Adv. Funct. Mater.* **2019**, *30*, 1906081.
(7) Wang, Y.; Li, J.; Wei, Z. Transition-Metal-Oxide-Based Catalysts for the Oxygen Reduction Reaction. *J. Mater. Chem. A* **2018**, *6*, 8194−8209.
(8) Zhao, S.; Wang, D.-W.; Amal, R.; Dai, L. Carbon-Based Metal-Free Catalysts for Key Reactions Involved in Energy Conversion and Storage. *Adv. Mater.* **2019**, *31*, 1801526.
(9) Wu, X.; Zhou, S.; Wang, Z.; Liu, J.; Pei, W.; Yang, P.; Zhao, J.; Qiu, J. Engineering Multifunctional Collaborative Catalytic Interface Enabling Efficient Hydrogen Evolution in All pH Range and Seawater. *Adv. Energy Mater.* **2019**, *9*, 1901333.
(10) Wu, Z. Y.; Xu, X. X.; Hu, B. C.; Liang, H. W.; Lin, Y.; Chen, L. F.; Yu, S. H. Iron Carbide Nanoparticles Encapsulated in Mesoporous Fe-N-Doped Carbon Nanofibers for Efficient Electrocatalysis. *Angew. Chem., Int. Ed.* **2015**, *54*, 8179−8183.
(11) Niu, S. S.; Wang, Z. Y.; Zhou, T.; Yu, M. L.; Yu, M. Z.; Qiu, J. S. A Polymetallic Metal-Organic Framework-Derived Strategy toward Synergistically Multidoped Metal Oxide Electrodes with Ultralong Cycle Life and High Volumetric Capacity. *Adv. Funct. Mater.* **2017**, *27*, 1605332.
(12) Wang, Q.; Lei, Y.; Chen, Z.; Wu, N.; Wang, Y.; Wang, B.; Wang, Y. Fe/Fe_3C@C Nanoparticles Encapsulated in N-Doped Graphene−CNTs Framework as an Efficient Bifunctional Oxygen Electrocatalyst for Robust Rechargeable Zn−Air Batteries. *J. Mater. Chem. A* **2018**, *6*, 516−526.
(13) Zhang, W.; Yao, X.; Zhou, S.; Li, X.; Li, L.; Yu, Z.; Gu, L. ZIF-8/ZIF-67-Derived Co-N_x-Embedded 1D Porous Carbon Nanofibers with Graphitic Carbon-Encased Co Nanoparticles as an Efficient Bifunctional Electrocatalyst. *Small* **2018**, *14*, 1800423.
(14) Wen, X.; Yang, X.; Li, M.; Bai, L.; Guan, J. Co/CoO_x Nanoparticles Inlaid onto Nitrogen-Doped Carbon-Graphene as a Trifunctional Electrocatalyst. *Electrochim. Acta* **2019**, *296*, 830−841.
(15) Bavykina, A.; Kolobov, N.; Khan, I. S.; Bau, J. A.; Ramirez, A.; Gascon, J. Metal−Organic Frameworks in Heterogeneous Catalysis: Recent Progress, New Trends, and Future Perspectives. *Chem. Rev.* **2020**, *16*, 8468.
(16) Konnerth, H.; Matsagar, B. M.; Chen, S. S.; Prechtl, M. H. G.; Shieh, F.-K.; Wu, K. C. W. Metal-Organic Framework (MOF)-Derived Catalysts for Fine Chemical Production. *Coordi. Chem. Rev.* **2020**, *416*, 213319.
(17) Hou, Y.; Huang, Y.-B.; Liang, Y.-L.; Chai, G.-L.; Yi, J.-D.; Zhang, T.; Zang, K.-T.; Luo, J.; Xu, R.; Lin, H.; Zhang, S.-Y.; Wang, H.-M.; Cao, R. Unraveling the Reactivity and Selectivity of Atomically Isolated Metal−Nitrogen Sites Anchored on Porphyrinic Triazine Frameworks for Electroreduction of CO_2. *CCS Chem.* **2019**, *1*, 384−395.
(18) Yu, M.; Zhou, S.; Wang, Z.; Pei, W.; Liu, X.; Liu, C.; Yan, C.; Meng, X.; Wang, S.; Zhao, J.; Qiu, J. A Molecular-Cage Strategy Enabling Efficient Chemisorption−Electrocatalytic Interface in Nanostructured Li_2S Cathode for Li Metal-Free Rechargeable Cells with High Energy. *Adv. Funct. Mater.* **2019**, *29*, 1905986.
(19) Xia, B. Y.; Yan, Y.; Li, N.; Wu, H. B.; Lou, X. W.; Wang, X. A Metal−Organic Framework-Derived Bifunctional Oxygen Electrocatalyst. *Nat. Energy* **2016**, *1*, 15006.
(20) Chen, H.; Shen, K.; Mao, Q.; Chen, J.; Li, Y. Nanoreactor of MOF-Derived Yolk−Shell Co@C−N: Precisely Controllable Structure and Enhanced Catalytic Activity. *ACS Catal.* **2018**, *8*, 1417−1426.
(21) Yi, J.-D.; Xu, R.; Wu, Q.; Zhang, T.; Zang, K.-T.; Luo, J.; Liang, Y.-L.; Huang, Y.-B.; Cao, R. Atomically Dispersed Iron−Nitrogen Active Sites within Porphyrinic Triazine-Based Frameworks for Oxygen Reduction Reaction in Both Alkaline and Acidic Media. *ACS Energy Lett.* **2018**, *3*, 883−889.
(22) Meng, J.; Liu, X.; Niu, C.; Pang, Q.; Li, J.; Liu, F.; Liu, Z.; Mai, L. Advances in Metal−Organic Framework Coatings: Versatile Synthesis and Broad Applications. *Chem. Soc. Rev.* **2020**, *49*, 3142−3186.
(23) Lai, Q.; Zhu, J.; Zhao, Y.; Liang, Y.; He, J.; Chen, J. MOF-Based Metal-Doping-Induced Synthesis of Hierarchical Porous Cu-N/C Oxygen Reduction Electrocatalysts for Zn−Air Batteries. *Small* **2017**, *13*, 1700740.
(24) Zhang, S. L.; Guan, B. Y.; Lou, X. W. Co−Fe Alloy/N-Doped Carbon Hollow Spheres Derived from Dual Metal−Organic Frameworks for Enhanced Electrocatalytic Oxygen Reduction. *Small* **2019**, *15*, 1805324.
(25) Zhang, M.; Dai, Q.; Zheng, H.; Chen, M.; Dai, L. Novel MOF-Derived Co@N-C Bifunctional Catalysts for Highly Efficient Zn−Air Batteries and Water Splitting. *Adv. Mater.* **2018**, *30*, 1705431.
(26) Liu, S.; Wang, Z.; Zhou, S.; Yu, F.; Yu, M.; Chiang, C.-Y.; Zhou, W.; Zhao, J.; Qiu, J. Metal−Organic-Framework-Derived Hybrid Carbon Nanocages as a Bifunctional Electrocatalyst for Oxygen Reduction and Evolution. *Adv. Mater.* **2017**, *29*, 1700874.
(27) Huang, L.; Zhang, X.; Han, Y.; Wang, Q.; Fang, Y.; Dong, S. In-Situ Synthesis of Ultrathin Metal−Organic Framework Nanosheets: a New Method for 2D Metal-Based Nanoporous Carbon Electrocatalysts. *J. Mater. Chem. A* **2017**, *5*, 18610−18617.
(28) Mahmood, A.; Guo, W.; Tabassum, H.; Zou, R. Metal-Organic Framework-Based Nanomaterials for Electrocatalysis. *Adv. Energy Mater.* **2016**, *6*, 1600423.
(29) Zou, L.; Hou, C.-C.; Liu, Z.; Pang, H.; Xu, Q. Superlong Single-Crystal Metal−Organic Framework Nanotubes. *J. Am. Chem. Soc.* **2018**, *140*, 15393−15401.
(30) Meng, J.; Liu, X.; Li, J.; Li, Q.; Zhao, C.; Xu, L.; Wang, X.; Liu, F.; Yang, W.; Xu, X.; Liu, Z.; Niu, C.; Mai, L. General Oriented Synthesis of Precise Carbon-Confined Nanostructures by Low-Pressure Vapor Superassembly and Controlled Pyrolysis. *Nano Lett.* **2017**, *17*, 7773−7781.
(31) Meng, J.; Li, J.; Liu, J.; Zhang, X.; Jiang, G.; Ma, L.; Hu, Z.-Y.; Xi, S.; Zhao, Y.; Yan, M.; Wang, P.; Liu, X.; Li, Q.; Liu, J. Z.; Wu, T.; Mai, L. Universal Approach to Fabricating Graphene-Supported Single-Atom Catalysts from Doped ZnO Solid Solutions. *ACS Cent. Sci.* **2020**, *6*, 1431−1440.
(32) Jiang, H.; Wang, Q.; Wang, H.; Chen, Y.; Zhang, M. Temperature Effect on the Morphology and Catalytic Performance of Co-MOF-74 in Low-temperature NH_3-SCR Process. *Catal. Commun.* **2016**, *80*, 24−27.
(33) Ammar, M.; Jiang, S.; Ji, S. Heteropoly Acid Encapsulated into Zeolite Imidazolate Framework (ZIF-67) Cage as an Efficient Heterogeneous Catalyst for Friedel−Crafts Acylation. *J. Solid State Electrochem.* **2016**, *233*, 303−310.
(34) Dietzel, P. D. C.; Morita, Y.; Blom, R.; Fjellvåg, H. An In-Situ High-Temperature Single-Crystal Investigation of a Dehydrated Metal−Organic Framework Compound and Field-Induced Magnetization of One-Dimensional Metal−Oxygen Chains. *Angew. Chem., Int. Ed.* **2005**, *44*, 6354−6358.
(35) Guo, J.; Gadipelli, S.; Yang, Y.; Li, Z.; Lu, Y.; Brett, D. J. L.; Guo, Z. An Efficient Carbon-Based ORR Catalyst from Low-Temperature Etching of ZIF-67 with Ultra-Small Cobalt Nanoparticles and High Yield. *J. Mater. Chem. A* **2019**, *7*, 3544−3551.
(36) Liang, Z.; Zhang, C.; Yuan, H.; Zhang, W.; Zheng, H.; Cao, R. PVP-Assisted Transformation of a Metal−Organic Framework into Co-Embedded N-Enriched Meso/microporous Carbon Materials as Bifunctional Electrocatalysts. *Chem. Commun.* **2018**, *54*, 7519−7522.
(37) Lu, Z.; Wang, B.; Hu, Y.; Liu, W.; Zhao, Y.; Yang, R.; Li, Z.; Luo, J.; Chi, B.; Jiang, Z.; Li, M.; Mu, S.; Liao, S.; Zhang, J.; Sun, X. An Isolated Zinc−Cobalt Atomic Pair for Highly Active and Durable Oxygen Reduction. *Angew. Chem., Int. Ed.* **2019**, *58*, 2622−2626.
(38) Wang, Y.; Wang, C.; Wang, Y.; Liu, H.; Huang, Z. Superior Sodium-Ion Storage Performance of Co_3O_4@nitrogen-doped Carbon: Derived from a Metal−Organic Framework. *J. Mater. Chem. A* **2016**, *4*, 5428−5435.
(39) Wang, K.; Chen, Y.; Tian, R.; Li, H.; Zhou, Y.; Duan, H.; Liu, H. Porous Co−C Core−Shell Nanocomposites Derived from Co-

https://dx.doi.org/10.1021/acsami.0c14112
ACS Appl. Mater. Interfaces XXXX, XXX, XXX−XXX

MOF-74 with Enhanced Electromagnetic Wave Absorption Performance. *ACS Appl. Mater. Interfaces* **2018**, *10*, 11333−11342.
(40) Hu, H.; Han, L.; Yu, M.; Wang, Z.; Lou, X. W. Metal−Organic-Framework-Engaged Formation of Co Nanoparticle-Embedded Carbon@Co_9S_8 Double-Shelled Nanocages for Efficient Oxygen Reduction. *Energy Environ. Sci.* **2016**, *9*, 107−111.
(41) Gao, H.; Li, Y.; Meng, E.; Ma, Y.; Zhang, Y.; Wang, L.; Luo, H.; Zhang, L.; Chen, W.; Xia, Y. Co/NC-Gr Composite Derived from ZIF-67: Effects of Preparation Method on the Structure and Electrocatalytic Performance for Oxygen Reduction Reaction. *Int. J. Hydrogen Energy* **2020**, *45*, 4403−4416.
(42) Wang, R.; Sun, P.; Yuan, Q.; Nie, R.; Wang, X. MOF-Derived Cobalt-Embedded Nitrogen-Doped Mesoporous Carbon Leaf for Efficient Hydrogen Evolution Reaction in Both Acidic and Alkaline Media. *Int. J. Hydrogen Energy* **2019**, *44*, 11838−11847.
(43) Yu, P.; Wang, L.; Sun, F.; Xie, Y.; Liu, X.; Ma, J.; Wang, X.; Tian, C.; Li, J.; Fu, H. Co Nanoislands Rooted on Co−N−C Nanosheets as Efficient Oxygen Electrocatalyst for Zn−Air Batteries. *Adv. Mater.* **2019**, *31*, 1901666.
(44) Wang, J.; Wang, Q.; She, W.; Xie, C.; Zhang, X.; Sun, M.; Xiao, J.; Wang, S. Tuning the Electron Density Distribution of the Co-N-C Catalysts through Guest Molecules and Heteroatom Doping to Boost Oxygen Reduction Adminctivity. *J. Power Sources* **2019**, *418*, 50−60.
(45) Luo, M.; Zhao, Z.; Zhang, Y.; Sun, Y.; Xing, Y.; Lv, F.; Yang, Y.; Zhang, X.; Hwang, S.; Qin, Y.; Ma, J.-Y.; Lin, F.; Su, D.; Lu, G.; Guo, S. PdMo Bimetallene for Oxygen Reduction Catalysis. *Nature* **2019**, *574*, 81−85.
(46) Xia, W.; Li, J.; Wang, T.; Song, L.; Guo, H.; Gong, H.; Jiang, C.; Gao, B.; He, J. The Synergistic Effect of Ceria and Co in N-Doped Leaf-Like Carbon Nanosheets Derived from a 2D MOF and Their Enhanced Performance in the Oxygen Reduction Reaction. *Chem. Commun.* **2018**, *54*, 1623−1626.
(47) Wang, M.-Q.; Ye, C.; Wang, M.; Li, T.-H.; Yu, Y.-N.; Bao, S.-J. Synthesis of M (Fe_3C, Co, Ni)-Porous Carbon Frameworks as High-Efficient ORR Catalysts. *Energy Stor. Mater.* **2018**, *11*, 112−117.
(48) Guo, D.; Shibuya, R.; Akiba, C.; Saji, S.; Kondo, T.; Nakamura, J. Active Sites of Nitrogen-Doped Carbon Materials for Oxygen Reduction Reaction Clarified Using Model Catalysts. *Science* **2016**, *351*, 361.
(49) Meng, J.; Niu, C.; Xu, L.; Li, J.; Liu, X.; Wang, X.; Wu, Y.; Xu, X.; Chen, W.; Li, Q.; Zhu, Z.; Zhao, D.; Mai, L. General Oriented Formation of Carbon Nanotubes from Metal−Organic Frameworks. *J. Am. Chem. Soc.* **2017**, *139*, 8212−8221.
(50) Deng, D.; Yu, L.; Chen, X.; Wang, G.; Jin, L.; Pan, X.; Deng, J.; Sun, G.; Bao, X. Iron Encapsulated within Pod-Like Carbon Nanotubes for Oxygen Reduction Reaction. *Angew. Chem., Int. Ed.* **2013**, *52*, 371−375.

https://dx.doi.org/10.1021/acsami.0c14112
ACS Appl. Mater. Interfaces XXXX, XXX, XXX−XXX